ГОДИШНИК НА УНИВЕРСИТЕТА ПО АРХИТЕКТУРА, СТРОИТЕЛСТВО И ГЕОДЕЗИЯ
СОФИЯ

Том 52 2019 Брой 2
Volume Issue

ANNUAL OF THE UNIVERSITY OF ARCHITECTURE, CIVIL ENGINEERING AND GEODESY
SOFIA

Получена: 01.12.2018 г.
Приета: 22.03.2019 г.

MAGNETIC, ELECTRIC AND PHONON PROPERTIES OF PURE AND ION-DOPED MULTIFERROIC HfO_2 NANOPARTICLES

A. Apostolov[1], I. Apostolova[2], J. Wesselinowa[3]

Keywords: *HfO_2 nanoparticles, magnetization, polarization, phonon energy, ion doping, microscopic model*

ABSTRACT

The magnetic, electric and phonon properties of pure and ion-doped HfO_2 nanoparticles are investigated theoretically using a microscopic model taking into account the spin-phonon interactions. By doping with Dy ions we observe a decrease whereas doping with Ni leads to increase of the magnetization M. A maximum in M for Y dopants at x = 10% is obtained. This is due to the different radii of the doping ions compared to the Hf ions as well as to the oxygen vacancies which appear by the doping process. The polarization P decreases with the temperature T. It has a kink at T_N. P increases with decreasing nanoparticle size. The polarization is calculated for different dopant concentrations, it has a maximum at small x values. The phonon energy decreases whereas the damping increases with increasing T. By different ion doping the energy can increase or decrease. The damping always increases with x. We have also studied the size and doping dependence of the band gap energy in HfO_2 nanoparticles.

1. Introduction

Wide band gap oxide based diluted magnetic semiconductors (DMS) doped with transition metal (TM) ions have been studied due to number of unusual electronic and magnetic

[1] Angel Apostolov, Assoc. Prof. Dr., Dpt. "Physics", UACEG, 1 H. Smirnenski Blvd., Sofia 1046, e-mail: angelapos@abv.bg
[2] Iliana Apostolova, Assoc. Prof. Dr., Dpt. "Mathematics and Physics", University of Forestry, 10 Kl. Ohridsky Blvd., Sofia 1756, e-mail: inaapos@abv.bg
[3] Julia Wesselinowa, Prof. D.Sc., Dpt. "Solid state physics", University of Sofia, 5 J. Bouchier Blvd., Sofia 1164, e-mail: julia@phys.uni-sofia.bg

properties. Recently, room-temperature ferromagnetism (RTFM) has been observed in undoped semiconducting TiO_2, SnO_2, CeO_2, HfO_2 nanostructures due to uncompensated spins or to oxygen vacancies at the surface [1 – 5]. Nanosized metal-oxide semiconductors such as HfO_2 are currently attracting academic and industrial community due to its unique combination of properties. HfO_2 has three crystalline phases at atmosphere pressure, monoclinic, the only stable phase at room temperature [6], tetragonal at approximately ~ 1700 °C and a cubic phase at ~ 2600 °C [7].

Stabilization of tetragonal and cubic phase of HfO_2 in ambient conditions can be obtained with doping by different methods of preparation and heat treatment [8]. Using density functional theory, Lee et al. [9] predicted that while dopants such as Si, Ge, Sn, P, Al or Ti having ionic radii smaller than Hf favour the tetragonal phase, dopants like Y, Gd or Sc with larger ionic radii stabilize the cubic phase of HfO_2 at room temperature. The substitution of Hf with larger cations thus obviously increases the lattice volume resulting in a more stable cubic phase. For spintronic applications, it is desirable to have a material in which the magnetic metallic ions are diluted in a semiconductor lattice. This can be achieved by doping a non-magnetic semiconductor (e.g., HfO_2) with a TM element (e.g., Fe, Ni, Co) allowing the occurrence of a spin polarized current while still exhibiting all of the basic functions of an undoped matrix [10 – 14]. The magnetization M_s increases with increasing Ni content [11] and decreases with increasing of Dy doping [7]. Kumar et al. [7] have shown that while the Neel temperature (T_N) for $x = 0$ in Dy doped HfO_2 NPs is found to be 45.5 K, for $x = 0.05$, 0.07 and 0.11, T_N decreases to 4.6, 2.8 and 2.5 K, respectively. The doping effects with rare earth (RE) ions (Y, Dy, Ce, Sm, Eu) on the magnetic properties [7, 15 – 18] are also studied. To obtain the desired results it is necessary that the dopant atoms must be evenly dissolved in the host lattice and the resulting ferromagnetism indeed originates from the doped matrices.

The group theoretical analysis of mode symmetry by Anastassakis et al. [19] predicts 18 Raman-active modes (A_g and B_g), 15 infrared-active modes, and 3 acoustic modes. First-principles calculations were performed to obtain a better understanding of the vibration modes [20 – 23]. Li et al. [24] have measured Raman spectra of monoclinic HfO_2 at temperatures up to 1100 K. Raman peak shifts and broadenings are reported. Phonon dynamics calculations were performed with the shell model. Galvez-Barboza et al. [25] and Mendoza-Mendoza et al. [26] have studied the Raman spectra of Ce^{-3} doped HfO_2 nanoparticles (NPs). Sharma et al. [11] have observed that in Ni doped HfO_2 NPs as the concentration of Ni increases the HfO_2 phonon mode shifted to lower frequencies. Jayaraman et al. [27] have shown that the Raman peaks in HfO_2 NPs are shifted to higher frequencies compared to bulk HfO_2. To date the assignment of Raman peaks of HfO_2 has not been fully convincing. Recently, in HfO_2 pure and doped nanostructures ferroelectricity is observed [28 – 35]. The ferroelectric HfO_2 can be applied for ferroelectric random-access memories and ferroelectric field-effect transistors [36]. From first principles, Barabash [37] predicts several, yet unknown, low-energy, dynamically stable phases of HfO_2. One of the predicted metastable phases has a finite ferroelectric polarization and could be potentially responsible for the ferroelectric and/or antiferroelectric behavior recently reported in thin $(Hf,Zr)O_2$-based films. The origin of ferroelectricity in $Hf_{1-x}Zr_xO_2$ is studied by Materlik et al. [38] using a computational investigation and a surface energy model. First-principles calculations are used to study the effects of neutral and 2+ charged oxygen vacancies on the dielectric properties of crystalline HfO_2 by Cockayne [39].

In the present paper, by using a microscopic model we will investigate the magnetic, electric and phonon properties of pure and TM and RE doped HfO_2 NPs. We will connect the exchange interaction parameters with the changes of the lattice parameters due to the different ionic radius of the dopants.

2. Model and Method

The Hamiltonian of a HfO_2 NP for the magnetic subsystem taking into account the spin-phonon interaction is given by:

$$H_m = H_{sp} + H_{sp-ph}. \tag{1}$$

The magnetic properties are analyzed using the Heisenberg model for the Hf-ions with different valence states on the surface:

$$H_{sp} = -\sum_{i,j} J_{ij}\left(S_i^+ S_j^- + S_i^z S_j^z\right) - \sum_i D_i\left(S_i^z\right)^2, \tag{2}$$

where S_i is the Heisenberg spin-operator for the localized spins at site *i*. J_{ij} is the exchange integral between neighboring sites *i* and *j* of the Hf-ions, $D_i < 0$ is the single-site anisotropy parameter ($| D_i | << J_{ij}$). The NP is defined by fixing the origin at a certain Hf-ion in the center of the particle and including all other Hf-ions within the particle into shells. The shells are numbered by $n = 0, ..., N$, where $n = 0$ denotes the central ion and $n = N$ represents the surface shell of the system. In order to explain the experimentally observed connection between the lattice distortion and the magnetism in doped DMS NPs [40 – 42] we must take into account the anharmonic spin-phonon interaction $H_{sp\text{-}ph}$:

$$H_{sp-ph} = \frac{1}{2}\sum_{i,j} \bar{F}(i,j) Q_i S_j^z - \frac{1}{4}\sum_{i,j,r} \bar{R}(i,j,r) Q_i Q_j S_r^z + hc. \tag{3}$$

$\bar{F}$ and $\bar{R}$ designate the amplitudes for coupling of phonons to the spin excitations in first and second order, respectively.

H_{ph} contains the lattice vibrations including anharmonic phonon-phonon interactions:

$$H_{ph} = \frac{1}{2!}\sum_i \omega_{0i} a_i a_i^+ + \frac{1}{3!}\sum_{i,j,r} B(i,j,r) Q_i Q_j Q_r + \frac{1}{4!}\sum_{i,j,r,s} A(i,j,r,s) Q_i Q_j Q_r Q_s, \tag{4}$$

where Q_i and ω_{0i} are the normal coordinate and frequency, respectively, of the lattice mode.

The ferroelectric properties are described by the Ising model in a transverse field:

$$H_e = -\Omega\sum_i B_i^x - \frac{1}{2}\sum_{i,j} \bar{J}_{ij} B_i^z B_j^z, \tag{5}$$

where B_i^x, B_i^z are the spin-1/2 operators of the pseudo-spins, $\bar{J}_{ij} > 0$ denotes the nearest-neighbor pseudo-spin interaction, Ω is the tunnelling frequency. According to Clima [43] we assume as the simplest model that the four O ions switch the polarization in the HfO_2 unit cell by jumping in the same *c* direction over the potential barrier in a double-well potential. In the ordered phase we have the mean values $\langle S^x \rangle \neq 0$ and $\langle S^z \rangle \neq 0$, and it is appropriate to choose a new coordinate system rotating the original one used in (5) by the angle θ in the *xz* plane. The rotation angle θ is determined by the requirement $S^{x'} = 0$ in the new coordinate system.

In principle the coexistence of spontaneous electric polarization and a finite saturation magnetization could give rise to a multiferroic behavior such as in the HfO_2 NPs. The full Hamiltonian $H = H_e + H_m + H_{me}$ must include a coupling magnetoelectric term H_{me}. We assume a biquadratic magnetoelectric coupling *g* between the two order parameters due to the fact that $T_C >> T_N$ [44]:

$$H_{me} = -g\sum_{i,j,k,l} B_i^z B_j^z S_k S_l \ . \tag{6}$$

To obtain the analytically expressions for the magnetization and the magnetic excitations we define the following Green's function:

$$G_{ij}(t) = -i\theta(t)\left\langle\left[S_i^+(t), S_j^-\right]\right\rangle = \left\langle\left\langle S_i^+(t), S_j^-\right\rangle\right\rangle. \tag{7}$$

The relative magnetization M is observed from:

$$M = \left\langle S^z\right\rangle = \frac{1}{N}\sum_n\left[(S+0.5)\coth[(S+0.5)\beta E_n] - 0.5\coth(0.5\beta E_n)\right], \tag{8}$$

where N is the number of shells, $\beta = 1/k_BT$, k_B is the Boltzmann constant, T is the absolute temperature. E_n are the elementary spin excitations of a given shell. For the spin excitation energy we obtain the following expression:

$$\begin{aligned} E_{ij} = \Bigg(\frac{2}{N'}\sum_m J_{im}^{eff}\left(\left\langle S_m^- S_i^+\right\rangle + 2\left\langle S_m^z S_i^z\right\rangle\right)\delta_{ij} - 2J_{ij}^{eff}\left(\left\langle S_i^- S_j^+\right\rangle + 2\left\langle S_i^z S_j^z\right\rangle\right) + \\ +2D_i\left(2\left\langle S_m^z S_i^z\right\rangle - \left\langle S_i^- S_j^+\right\rangle\right)\delta_{ij} + 2g\mu_B H\left\langle S_i^z\right\rangle\delta_{ij}\Bigg)\Big/ 2\left\langle S_i^z\right\rangle\delta_{ij}, \end{aligned} \tag{9}$$

where N' is the number of lattice sites. J^{eff} is the renormalized spin-spin exchange interaction constant due to the spin-phonon interactions F and R and the magnetoelectric coupling g:

$$J^{eff} = J + \frac{2F^2}{\omega_0 - MR} + 2gP^2\cos^2\theta \ . \tag{10}$$

The approximation which is used by the numerical calculation is the following: in Equation (9) we have taken into account the transverse correlation functions, which are obtained from the Spectral theorem, and have decoupled the longitudinal ones: $\langle S_i^z S_j^z\rangle \to \langle S_i^z\rangle\langle S_j^z\rangle$.

We have calculated the polarization in a HfO_2 NP from the Green's function $g_{ij} = \langle\langle B_i^+; B_j^-\rangle\rangle$:

$$P_i = \frac{1}{2N'}\sum_j \tanh\frac{\bar{E}_{ij}}{2k_BT}, \tag{11}$$

where $\bar{E}_{ij}$ is the transverse pseudo-spin wave energy:

$$\begin{aligned} E_{ij} = 2\Omega\sin\theta + \frac{1}{2}P_i\cos^2\theta\bar{J}_i^{eff} - \frac{1}{4}P_i\sin^2\theta\bar{J}_i^{eff} - \\ -\frac{1}{N'P_i}\sum_j\left(\cos^2\theta\bar{J}_{ij}^{eff} - \frac{1}{2}\sin^2\theta\bar{J}_{ij}^{eff}\right)\left\langle B_i^- B_j^+\right\rangle, \end{aligned} \tag{12}$$

with $\sin\theta = 4\Omega/\left(P\bar{J}^{eff}\right)$ and $\bar{J}^{eff} = J_0 + 2g\left(\left\langle S^-S^+\right\rangle + \left\langle S^z\right\rangle^2\right)$.

The phonon energy is observed from the full Hamiltonian taking into account the anharmonic spin-phonon interactions F and R and the phonon-phonon interactions A and B:

$$\omega_{ij}^2 = \omega_0^2 - 2\omega_0 \left(M_i M_j R_{ij} \delta_{ij} - \frac{1}{2N'} \sum_r A_{ijr} \left(2\bar{N}_r + 1 \right) - B_{ij} \left\langle Q_{ij} \right\rangle \delta_{ij} \right), \tag{13}$$

with

$$\left\langle Q_{ij} \right\rangle = \frac{M_i M_j F_{ij} \delta_{ij} - \frac{1}{N'} \sum_r B_{ijr} \left(2\bar{N}_r + 1 \right)}{\omega_0 - M_i M_j R_{ij} \delta_{ij} - \frac{1}{N'} \sum_r A_{ijr} \left(2\bar{N}_r + 1 \right)}. \tag{14}$$

M_i is the magnetization at site i.

The phonon damping is also calculated using the method of Tserkovnikov [45]. All equations must be calculated self-consistently.

3. Numerical Results and Discussion

Undoped oxide NPs exhibit RTFM due to surface oxygen vacancies. The model parameters for an undoped HfO_2 NP with an icosahedral symmetry are: J_{0b} = 0.25 meV, D_b = -0.1 meV, F_b = 4 cm^{-1}, R_b = -0.35 cm^{-1}, S = 1/2, $J_s = 0.6J_b$, the phonon energy of the A_g mode is ω_0 = 149 cm^{-1}.

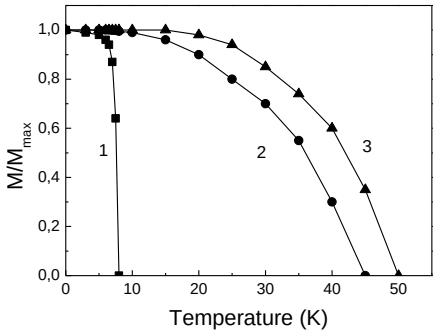

Figure 1. Temperature dependence of the magnetization M/Mmax for pure (2), Dy doped (1) and Ni doped (3) HfO_2 NPs (x = 2%) with different J_d^{eff} / J_b^{eff} : (1) 0.2, (2) 1, (3) 1.2

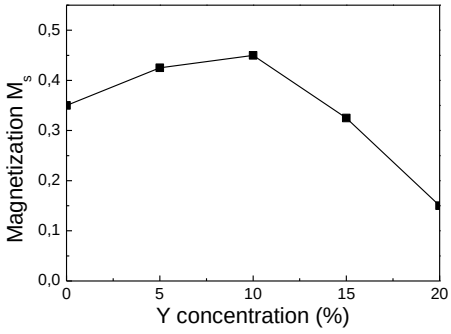

Figure 2. Y concentration dependence of the magnetization in HfO_2 NPs, T = 30 K and N = 5

Firstly, we consider the spontaneous magnetization M_s in pure HfO_2 NPs. With increasing temperature, M_s decreases (Fig. 1). The magnetic phase transition temperature is 45 K. Doping with different ions can change the magnetization in HfO_2 NPs (Fig. 1, curve 2). We can see that by doping with Ni ions M_s is larger compared to the undoped case (Fig. 1, curve 3), whereas by Dy doping we have the opposite case – M_s is smaller (Fig. 1, curve1) than in the undoped case. This is in good qualitative agreement with the experimental data for Ni doping [11] and for Dy doping [7]. This is due to the different radii of Ni and Dy doping ions. The Ni ions, which have a valence close to 2+ [11], are smaller compared to the Hf ions, i.e. we have a compressive strain, which leads to enhanced exchange interaction constant J^{eff} and

larger magnetization. The Dy ions are larger compared to the host Hf ions; this is connected with a tensile strain, with smaller value of J^{eff} and smaller magnetization. By the doping in some cases we have a maximum value in the magnetization curve. For example, by Y dopants we observe a maximum in $M_s(x)$ at x = 10% (see Fig. 2) in agreement with the experimental data of Ref. [16]. The increase of the magnetization with increasing Y dopant concentration x can be understood in terms of oxygen vacancies created to retain charge neutrality of HfO_2 matrix as some Ni ions that replace Hf^{4+}, resulting in ferromagnetic interactions at lower concentrations. By higher Y concentration the oxygen vacancies increase stronger and this leads to antiferromagnetic interactions and the magnetization begins to decrease.

As mentioned above, in the last years ferroelectricity is reported in HfO_2 NPs by many authors [28 – 35]. Therefore we have calculated the polarization P in dependence on temperature (Fig. 3) and doping concentration (Fig. 4). With increasing temperature T the polarization P decreases and vanishes at the Curie temperature T_C = 723 K [29] which is much higher in comparison with the magnetic phase transition temperature T_N = 45.5 K. This means that the two magnetic and ferroelectric orderings have independent mechanisms. In particular, this generally leads to different transition temperatures for the two subsystems. The model with biquadratic coupling between the pseudospins and the magnetic moments can be applied to multiferroic substances where $T_C >> T_N$, for example in hexagonal $RMnO_3$ and $BiFeO_3$ [44, 46]. It can be seen that at the critical magnetic temperature T_N = 45 K there is a kink in the polarization which is due to the ME effect. At this temperature the magnetization in the multiferroic HfO_2 NP vanishes. Unfortunately, there are no experimental data which conform this effect in our $P(T)$-curve.

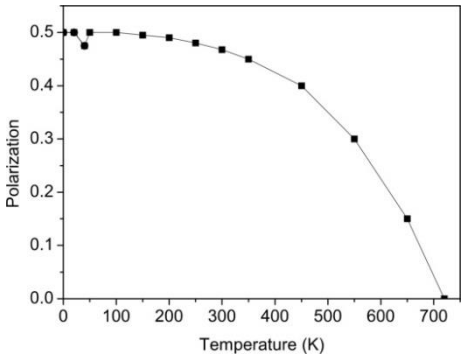

Figure 3. Temperature dependence of the polarization for a pure HfO_2 NP

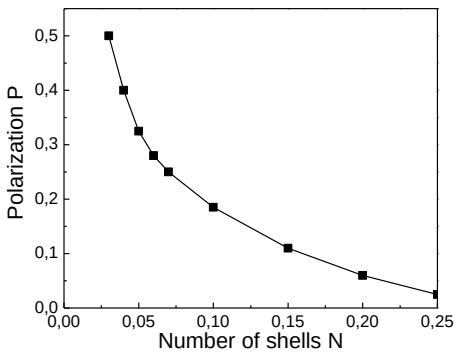

Figure 4. Size dependence of the polarization for a pure HfO_2 NP, T = 100 K

It must be mentioned that the polarization increases with decreasing particle size (see Fig. 4) with $J_s > J_b$. This is in agreement with the experimental data of Starschich and Boettger [30], and Shiraishi et al. [47].

Doping with different ions leads to changes in the polarization in comparison with the undoped case. Therefore we have calculated P for Al and Y doped HfO_2 NPs. The results are presented in Fig. 5. It can be seen that the polarization firstly increases with increasing dopant concentration. This is due to the enhanced oxygen vacancies and the ferromagnetic exchange interactions. Moreover, the radius of the doping Al ion is much smaller than that of the host ion Hf, we have a compressible strain, the exchange interaction J is enhanced, through the ME coupling the pseudospin interaction constant and the polarization, too. Then at a critical x value P reaches a maximum value and begins to decrease. With a further increase of the oxygen vacancies, by increasing the dopant concentration, there appears antiferromagnetic interaction,

i.e. the exchange interaction constants decrease and trough the magnetoelectric coupling also the polarization *P*. This discussion could be applied also for Y doping. A similar behaviour is reported by Mueller et al. [48, 49] in Al and Y doped HfO_2 NPs, respectively.

The peaks observed in the Raman spectrum of monoclinic HfO_2 NPs at 110, 133, 149, 256, 383, 500, 579 and 671 cm^{-1} could be assigned to the A_g modes [6, 50]. We consider the temperature dependence of the mode A_g = 149 cm^{-1} with a negative anharmonic spin-phonon interaction constant $R < 0$. We obtain a decreasing of the phonon energy with increasing temperature (Fig. 6) whereas the phonon damping increases with increasing *T* (Fig. 6). Such a softening of the A_g mode and broadening of this peak is reported by Li et al. [51]. The broadening of the A_g mode could be correlated with increasing O vacancy concentration by doping because this mode is very sensitive to disorder in oxygen sub-lattice. We observe that the phonon energy, i.e. the Raman peak value, is shifted to higher frequencies compared to the bulk monoclinic HfO_2 [51], which is in agreement with the results of Jayaraman et al. [27].

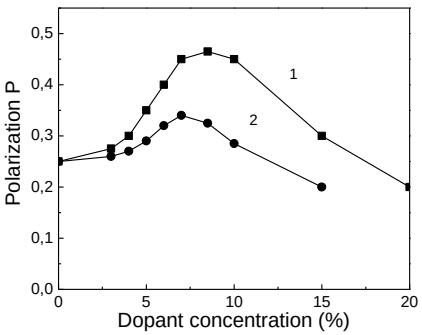

Figure 5. Dopant concentration dependence of the polarization for a Al (1) and Y (2) doped HfO_2 NP

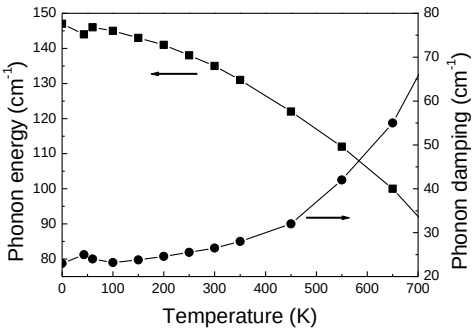

Figure 6. Temperature dependence of the phonon energy and damping for a pure HfO_2 NP

Now we will investigate the inuence of different ion doping on the phonon energy. The doping with Ni^{3+} or Al^{3+} ions in HfO_2 leads to increasing of the phonon frequency (see Fig. 7, curve 2). It should be noted that the ionic radius of Ni^{3+} (70 pm) or Al^{4+} (68 pm) ions is smaller than that of Hf^{4+} ion (85 pm) [32, 52]. The lattice parameters of Ni doped HfO_2 are also measured to decrease with increasing Ni dopants by Sharma et al. [11]. There appears a compressive strain, which leads in our model to increase of the exchange interaction and the spin-phonon interaction in the defect states due to the decreasing lattice parameters by the Al substitution. This means that we have to calculate the phonon energy with the following relation between the exchange interaction and spin-phonon constants in the defective and in the indefective states $|J_d| > |J_b|$, $|R_d| > |R_b|$.

By doping with Y or Gd ions we obtain the opposite behaviour – a decrease of the phonon energy with increasing dopant concentration (see Fig. 7, curve 1). The ionic radius of Gd^{3+} (108 pm) or Y^{3+} (104 pm) ion is larger compared to that of the Hf^{4+} ion [32].This means that we have a tensile strain which is connected in our investigations with decrease of the exchange interaction and anharmonic spin-phonon constants, i.e. we use the relation $|J_d| < |J_b|$, $|R_d| < |R_b|$. This leads to a decrease of the phonon energy (Fig. 7, curve 1). A similar behaviour we observe also for Eu doping. The lattice parameters of Eu doped HfO_2 increase because the ionic radius of Eu^{3+} (101 pm) is larger than the Hf one [53]. The effect of strain and oxygen deficiency on the Raman spectrum of monoclinic HfO_2 is investigated theoretically using first-principles calculations by Gao et al. [56]. 1% in-plane compressive strain applied to *a* and *c* axes is found to blue shift the phonon frequencies, while 1% tensile strain does the opposite.

Our calculations have shown that the phonon damping grows always with the dopant concentration whether the energy increases or decreases. The results are presented in Fig. 8, curves 1 and 2, and are in agreement with many authors. The phonon damping increases, i.e. the Raman modes are broadened due to the increased oxygen vacancy concentration when HfO_2 is doped with trivalent ions like Y [57]. With further increase of the Y content the Raman modes become broader implying that oxygen vacancy concentration further increases.

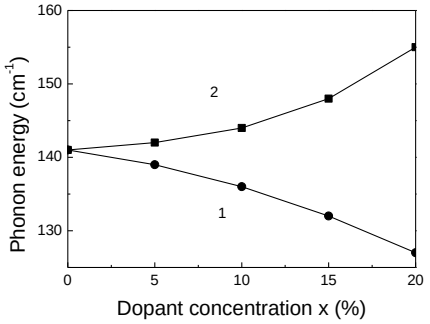

Figure 7. Dopant concentration dependence of the phonon energy in ion doped HfO_2 NP, T = 200 K: (1) Y, (2) Ni

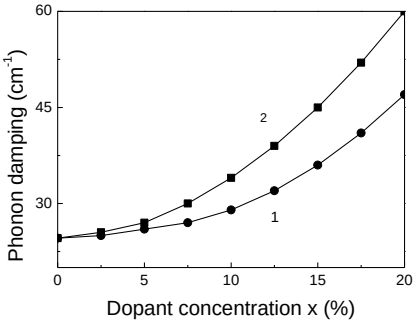

Figure 8. Dopant concentration dependence of the phonon damping in ion doped HfO_2 NP, T = 200 K: (1) Y, (2) Ni

Finally, we have calculated and discussed the band gap energy for pure and ion doped HfO_2 NPs. To be able to do this we need an extension of our model, namely we need the s-d model:

$$H_{s-d} = H_{sp} + H_{el} + H_{sp-el} + H_{el-ph}\,. \tag{15}$$

H_{sp} is the Heisenberg model for the *d*-electrons (see eq. 2).

H_{el} represents the usual Hamiltonian of the conduction band electrons:

$$H_{el} = \sum_{ij\sigma} t_{ij} c_{i\sigma}^{+} c_{j\sigma}\,, \tag{16}$$

where t_{ij} is the hopping integral, $c_{i\sigma}^{+}$ and $c_{i\sigma}$ are Fermi-creation and – annihilation operators.

$H_{sp\text{-}el}$ couples the two subsystems – Eqs. (2) and (16) – by an intra-atomic exchange interaction I_i:

$$H_{sp-el} = \sum\nolimits_i I_i S_i s_i\,. \tag{17}$$

The spin operators s_i of the conduction electrons at site i can be expressed as $s_i^{+} = c_{i+}^{+} c_{i-}$, $s_i^{z} = (c_{i+}^{+} c_{i+} - c_{i-}^{+} c_{i-})/2$.

$H_{el\text{-}ph}$ represents the interaction between the electron and the phonon subsystems which plays an important role in HfO_2 NPs [58 – 60]:

$$H_{el-ph} = i\sum\nolimits_{jk\sigma} A(ijk) c_{i\sigma}^{+} c_{j\sigma} \left(a_k^{+} - a_k\right) + hc\,, \tag{18}$$

where a_k^+ and a_k are phonon creation and annihilation operators, $A(ijk) = A'(\omega_k/2V)^{1/2}$ is the electron-phonon interaction constant.

In order to obtain the electronic energy ω_σ we define the following Green's function $g_{ij\sigma} = c_{i\sigma}; c_{i\sigma}^+$. The equation of motion is:

$$\left(\omega_\sigma - \sigma 0.5\left\langle s_i^z\right\rangle I_i \left\langle S_i^z\right\rangle + \frac{2A^2}{\omega_0}\left\langle n_\sigma\right\rangle\right) g_{ij\sigma}(\omega) = \delta_{ij} + \sum\nolimits_\delta t_{i,i+\delta} g_{i+\delta,j\sigma}(\omega). \tag{19}$$

$\langle s_n^z\rangle$ is the conduction-electron magnetization in the n-th shell:

$$\left\langle s_n^z\right\rangle = 0.5\left(\left\langle n_+\right\rangle - \left\langle n_-\right\rangle\right), \tag{20}$$

where $\langle n_+\rangle$ and $\langle n\_\rangle$ are the numbers of conduction electrons in the spin-up and spin-down bands, respectively.

The band gap energy is calculated from the equation [61, 62]:

$$E_g = \omega_+(k=0) - \omega_-\left(k = k_\sigma\right), \tag{21}$$

with ω_σ from Eq. (19).

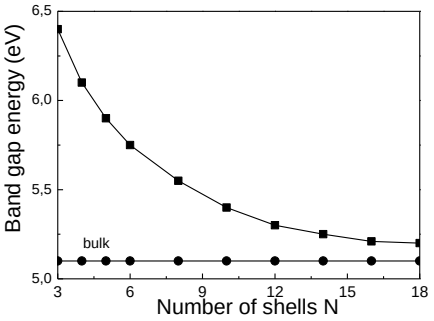

Figure 9. Size dependence of the band gap energy in HfO_2 NPs, T = 300 K

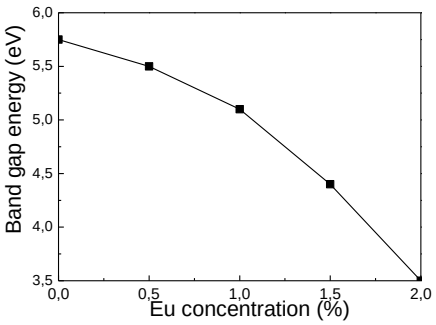

Figure 10. Dependence of the band gap energy on the Eu concentration in Eu doped HfO_2 NPs, T = 300 K and N = 6

The experimental band gap values for HfO_2 are in the range from 5.1 to 5.95 eV [53 – 55, 63 – 66]. The values are different for the different phases of HfO_2 – monoclinic, tetragonal and cubic. Moreover, the E_g values change for different intensities of laser irradiation and after thermal annealing, which can be explained in terms of a dimensional factor [67]. We take the value of the band gap of bulk cubic HfO_2 to be 5.1 eV [68]. The size dependence of E_g of monoclinic HfO_2 NP is calculated taking into account the electron-phonon interaction. The result is shown in Fig. 9. It can be seen that the band gap E_g increases strongly with decreasing particle size due to size effects. For a NP with N = 3 shells we obtain E_g = 6.4 eV. This is in good qualitative agreement with the experimental data of Jayaraman et al. [27].

We have calculated also the band gap in Eu^{3+} doped HfO_2 NPs. The band gap energy dependence on the Eu concentration is demonstrated in Fig. 10. E_g decreases with increasing

Eu doping concentration in agreement with the experimental data of Venkatachalam et al. [69]. The *d* states of the Eu ions and oxygen defects are mainly responsible for the narrowing of the band gap of HfO_2 NPs. This decrease of E_g is due also to the strong s-d interaction between the band electrons and the localized electrons and to the strong electron-phonon interaction. In principle, band gap shifts can be understood as the net result of two competing mechanisms: a widening due to the Burstein-Moss effect, and a narrowing due to electron-electron and electron-ion scattering.

4. Conclusion

On the basis of a microscopic model, taking into account the anharmonic spin-phonon and phonon-phonon interactions and using the Green's function theory, we have studied the magnetic, electric and phonon properties of pure and ion doped HfO_2 nanoparticles. The magnetization M in pure HfO_2 nanoparticles is due to surface oxygen vacancies. The Hf ion appears in two valences Hf^{4+} and Hf^{3+}. By doping with Dy ions we observe a decrease whereas doping with Ni leads to an increase of M. A maximum in M for Y dopants at x = 10% is obtained. This is due to the different radii of the doping ions compared to the Hf ions as well as to the oxygen vacancies which appear by the doping process.

The polarization P decreases with the temperature. It has a kink at the magnetic phase transition temperature T_N. P increases with decreasing nanoparticle size. The polarization is also calculated for different dopant concentrations, for example Al and Y. It has a maximum at small x values.

The phonon energy decreases whereas the damping increases with increasing T. There is also a kink at T_N. This is an evidence for the multiferroic character of the HfO_2 nanoparticles. By different ion doping the phonon energy can increase (for example Ni,Al) or decrease (Y,Eu,Sm) due to the different relation between the anharmonic spin-phonon interaction in the defect state R_d and in the undoped state R_b. The damping always increases with x independent on the behaviour of the phonon energy.

We have also calculated the band gap energy E_g in HfO_2 NPs. It increases with decreasing NP size. E_g decreases with increasing the Eu dopant concentration in Eu doped HfO_2 NPs. All results are in good qualitative agreement with the experimental data.

5. Acknowledgement

The authors acknowledge support from Center for Research and Desing of the University of Architecture, Civil Engineering and Geodesy for the financial support (contract number BN204/17).

REFERENCES

1. *A. Sundaresan and C. N. R. Rao*. Nano Today **4**, 96 (2009).

2. *L. Zhang, S. Ge, Y. Zuo, B. Zhang and L. Xi*. J. Phys. Chem. C **114**, 7541 (2010).

3. *Y. Liu, Z. Lockman, A. Aziz and J. MacManus-Driscoll*. J. Phys.: Condens. Matter **20**, 165201 (2008).

4. *G. S. Chang, J. Forrest, E. Z. Kurmaev, A. N. Morozovska, M. D. Glinchuk, J. A. McLeod, A. Moewes, T. P. Surkova and N. H. Hong*. Phys. Rev. B **85**, 165319 (2012).

5. *M. Venkatesan, C. B. Fitzgerald and J. M. D. Coey*. Nature **430**, 630 (2014).

6. *A. Ramadoss and S. J. Kim*. J. All.&Comp. **544**, 115 (2012).

7. *S. Kumar, S. B. Raib and C. Rath*. Phys. Chem. Chem. Phys. **19**, 18957 (2017).

8. *J. Wang, H. P. Li and R. Steven*. J. Mater. Sci. **27**, 5397 (1992).

9. *C. K. Lee, E. Cho, H. S. Lee, C. S. Hwang and S. Han*. Phys. Rev. B **78**, 012102 (2008).

10. *F. Pan, C. Song, X. J. Liu, Y. C. Yang and F. Zeng*. Mater. Sci. Eng. R **62**, 1 (2008).

11. *M. K. Sharma, D. K. Mishra, S. Ghosh, D. Kanjilal, P. Srivastava and R. Chatterjee*. J. Appl. Phys. **110**, 063902 (2011).

12. *A. Pucci, G. Clavel, M.-G. Willinger, D. Zitoun and N. Pinna*. J. Phys. Chem. C **113**, 12048 (2009).

13. *J. Buha, D. Arcon, M. Niederberger and I. Djerdj*. Phys. Chem. Chem. Phys. **12**, 15537 (2010).

14. *W. Liu, M Liu, R. Zhang, R. Ma and H. Wang*. Appl. Phys. Lett. **111**, 172404 (2017).

15. *T. S. N. Sales, F. H. M. Cavalcante, B. Bosch-Santos, L. F. D. Pereira, G. A. Cabrera-Pasca, R. S. Freitas, R. N. Saxena, and A. W. Carbonari*. AIP Adv. **7**, 056315 (2017).

16. *Z. D. Dohcevic-Mitrovic, N. Paunovic, B. Matovic, P. Osiceanu, R. Scurtu, S. Askrabic and M. Radovic*. Ceram. Int. **41**, 6970 (2015).

17. *S. Kumar, S. B. Rai and Chandana Rath*. J. Appl. Phys. **123**, 055108 (2018).

18. *S. Stojadinovic, N. Tadic, A. Ciric and R. Vasilic*. Opt. Mater. **77**, 19 (2018).

19. *E. Anastassakis, B. Papanicolaou and I. M. Asher*. J. Phys. Chem. Solids **36**, 667 (1975).

20. *X. Zhao and D. Vanderbilt*. Phys. Rev. B **65**, 233106 (2002).

21. *A. A. Demkov*. phys. stat. sol. (b) **226**, 57 (2001).

22. *R. Wu, B. Zhou, Q. Li, Z. Y. Jiang, W. B. Wang, W. Y. Ma and X. D. Zhang*. J. Phys. D: Appl. Phys. **45**, 125304 (2012).

23. *B. Zhou, H. Shi, X. D. Zhang, Q. Su and Z. Y. Jiang*. J. Phys. D: Appl. Phys. **47**, 115502 (2014).

24. *C. W. Li, M. M. McKerns and B. Fultz*. Phys. Rev. B **80**, 054304 (2009).

25. *S. Galvez-Barboza, L. A. Gonzalez, B. A. Puente-Urbina, E. M. Saucedo-Salazar and L. A. Garca-Cerda*. J. All.&Comp. **643**, S62 (2015).

26. *E. Mendoza-Mendoza, J. S. Quintero-Garca, B. A. Puente-Urbina, O. S. Rodrguez-Fernandez and L. A. Garca-Cerda*. J. All.&Comp. **692**, 448 (2017).

27. *V. Jayaraman, S. Sagadevan and R. Sudhakar*. J. Electr. Mater. **46**, 4392 (2017).

28. *K. Lee, T. Y. Lee, S. M. Yang, D. H. Lee, J. Park and S. C. Chae*. Appl. Phys. Lett. **112**, 202901 (2018).

29. *T. Shimizu, K. Katayama, T. Kiguchi, A. Akama, T. J. Konno, O. Sakata and H. Funakubo*. Sc. Reports **6**, 32931 (2016).

30. *S. Starschich and U. Boettger*. J. Mater. Chem. C **5**, 333 (2017).

31. *A. Chouprik, S. Zakharchenko, M. Spiridonov, S. Zarubin, A. Chernikova, R. Kirtaev, P. Buragohain, A. Gruverman, A. Zenkevich and D. Negrov*. ACS Appl. Mater. Interfaces **10**, 8818 (2018).

32. *M. H. Park, T. Schenk, C. M. Fancher, E. D. Grimley, C. Zhou, C. Richter, J. M. LeBeau, J. L. Jones, T. Mikolajick and U. Schroeder*. J. Mater. Chem. C **5**, 4677 (2017)

33. *T. C. U. Tromm, J. Zhang, J. Schubert, M. Luysberg, W. Zander, Q. Han, P. Meuffels, D. Meertens, S. Glass, P. Bernardy and S. Mantl*. Appl. Phys. Lett. **111**, 142904 (2017).

34. *A. Onodera and M. Takesada*. Crystals **7**, 232 (2017).

35. *T. V. Perevalov, D. R. Islamov, V. A. Gritsenko and I. P. Prosvirin*. Nanotechn. **29**, 194001 (2018).

36. *T. Mikolajick, S. Slesazeck, M. H. Park and U. Schroeder*. Mater. Adv. Semicond. Memories **43**, 340 (2018).

37. *S. V. Barabash*. J. Comput. Electron. **16**, 1227 (2017).

38. *R. Materlik, C. Kuenneth and A. Kersch*. J. Appl. Phys. **117**, 134109 (2015).

39. *E. Cockayne*. Phys. Rev. B **75**, 094103 (2007).

40. *S. B. Oseroff and R. Calvo*. Phys. Rev. B **5**, 2474 (1972).

41. *J. Hays, A. Punnoose, R. Baldner, M. H. Engelhard, J. Peloquin and K. M. Reddy*. Phys. Rev. B **72**, 075203 (2005).

42. *K. C. Verma and R. K. Kantone*. J. Chem. Chem. Phys. **18**, 17565 (2016).

43. *S. Clima, D. J. Wouters, C. Adelmann, T. Schenk, U. Schroeder, M. Jurczak and G. Pourtois*. Appl. Phys. Lett. **104**, 092906 (2014).

44. *J. M. Wesselinowa and I. N. Apostolova*. J. Appl. Phys. **104**, 084108 (2008).

45. *Yu. A. Tserkovnikov*. Theor. Math. Phys. **7**, 511 (1971).

46. *J. M.Wesselinowa and St. Kovachev*. J. Appl. Phys. **102**, 043911 (2007).

47. *T. Shiraishi, K. Katayamaa, T. Yokouchia, T. Shimizuc, T. Oikawaa, O. Sakata, H. Uchida, Y. Imai, T. Kiguchi, T. J. Konnob and H. Funakubo*. Mater. Sc. Semicond. Proc. **70**, 235 (2017).

48. *S. Mueller, J. Mueller, A. Singh, S. Riedel, J. Sundqvist, U. Schroeder and T. Mikolajick*. Adv. Funct. Mater. **22**, 2412 (2012).

49. *J. Mueller, U. Schroeder, T. S. Boescke, I. Mueller, U. Boettger, L. Wilde, J. Sundqvist, M. Lemberger, P. Kuecher, T. Mikolajick and L. Frey*. J. Appl. Phys. **110**, 114113 (2011).

50. *A. Vinod, M. S. Rathore and N. S. Rao*. Vacuum **155**, 339 (2018).

51. *C. W. Li, M. M. McKerns and B. Fultz*. Phys. Rev. B **80**, 054304 (2009).

52. *U. Schroeder, E. Yurchuk, J. Mueller, D. Martin, T. Schenk, P. Polakowski, C. Adelmann, M. I. Popovici, S. V. Kalinin and T. Mikolajick*. Jpn. J. Appl. Phys. **53**, 08LE02 (2014).

53. *E. N. Ceron, G. R. Gattorno, J. Guzmn-Mendoza, M. Garca-Hipolito and C. Falcony*. Open J. Synth. Theory&Appl. **2**, 73 (2013).

54. *J. M. Khoshman and M. E. Kordesch*. Surf. Coatings Techn. **201**, 3530 (2006).

55. *L. Khomenkova, Y.-T. An, D. Khomenkov, X. Portier, C. Labbe and F. Gourbilleau*. Physica B **453**, 100 (2014).

56. *L. Gao, E. Yalon, A. R. Chew, S. Deshmukh, A. Salleo, E. Pop and A. A. Demkov*. J. Appl. Phys. **121**, 224101 (2017).

57. *M. Yashima, H. Takahashi, K. Ohtake, T. Hirose, M. Kakihana, H. Arashi, Y. Ikuma, Y. Suzuki and M. Yoshimura*. J. Phys. Chem. Solids **57**, 289 (1996).

58. *J. L. Gavartin, D. M. Ramo, A. Shluger and G. Bersuker*. ECS Trans. **3**, 277 (2006).

59. *H. Nakamura and Y. Asai*. Phys. Chem. Chem. Phys. **18**, 8820 (2016).

60. *S. Papernov, M. D. Brunsman, J. B. O;iver, B. N. Hoffman, A. A. Kozlov, S. G. Demos, A. Shvydky, F. H. M. Cavalcante, L.Yang, C. S. Menoni, B. Roshanzadeh, S. T. P. Boyd, L. A. Emmert and W. Rudolph*. Optics Express **26**, 17608 (2018).

61. *E. Goryachev, E. V. Kuzmin and S. G. Ovchinnikov*. J. Phys. C **15**, 1481 (1982).

62. *J. M. Wesselinowa*. phys. stat. sol. (b) **146**, K55 (1988).

63. *H. Jiang, R. I. Gomez-Abal, P. Rinke and M. Scheffler*. Phys. Rev. B **81**, 085119 (2010).

64. *J. Manikantan, H.B. Ramalingam, B. C. Shekar, B. Murugan, R. R. Kumar and J. S. Santhoshi*. Mater. Lett. **186**, 42 (2017).

65. *K. H. P. Kumar, S. Vidya, S. S. Kumar, C. Vijayakumar, S. Solomon and J. K. Thomasumar*. J. Asian Ceram. Soc. **3**, 64 (2015).

66. *S. M. Taur*. Int. Res. J. Sc.& Eng. Special Issue **A2**, 140 (2018).

67. *M. A. Pugachevskii and V. I. Pan_lov*. J. Appl. Spectr **81**, 649 (2014).

68. *J. I. Beltran, M. C. Munoz and J. Hafner*. New J. Phys. **10**, 063031 (2008).

69. *J. Venkatachalam, S. Ganesan and P. Aruna*. Int. J. ChemTech Res. **8**, 1131 (2015).

МАГНИТНИ, ЕЛЕКТРИЧНИ И ФОНОННИ СВОЙСТВА НА ЧИСТИ И ДОТИРАНИ МУЛТИФЕРОИЧНИ HfO_2 НАНОЧАСТИЦИ

А. Апостолов[1], И. Апостолова[2], Ю. Веселинова[3]

Ключови думи: *HfO_2 наночастици, намагнитване, поляризация, фононна енергия, дотиране, микроскопичен модел*

РЕЗЮМЕ

Магнитните, електричните и фононните свойства на чисти и дотирани HfO_2 наночастици са изучени теоретично. Използван е теоретичен модел с отчитане на спин-фононното взаимодействие. При дотиране с Dy намагнитеността M намалява, докато при дотиране с Ni нараства. Наблюдава се максимум в M при дотиране с Y при концентрация x = 10%. Тези ефекти се дължат, както на различните радиуси на дотиращите йони спрямо Hf йони, така и на кислородните ваканции, които се появяват при процеса на дотиране. Поляризацията P намалява с увеличаване на температурата T, като се наблюдава аномалия около T_N. P нараства с намаляване на размера на наночастиците. Поляризацията е пресметната при различна концентрация на примесите, като се наблюдава максимум при малки стойности на x. С увеличаване на температурата T фононната енергия намалява, докато затихването се увеличава. При дотиране с различни йони фононната енергия може да нараства или намалява. Затихването винаги нараства с увеличаване на x. Изучена е също и зависимостта на ширината на зоната от дотирането и размера на HfO_2 наночастици.

[1] Ангел Апостолов, доц. д-р, кат. „Физика“, УАСГ, бул. „Хр. Смирненски“ 1, 1046 София, e-mail: angelapos@abv.bg

[2] Илиана Апостолова, доц. д-р, кат. „Математика и физика“, Лесотехнически университет, бул. „Кл. Охридски“ 10, 1756 София, e-mail: inaapos@abv.bg

[3] Юлия Веселинова, проф. дфн, кат. „Физика на твърдото тяло“, Софийски университет, бул. „Дж. Баучър“ 5, 1164 София, e-mail: julia@phys.uni-sofia.bg